A long-term neutral density database using commercial satellite data for atmospheric model calibration

Vishal Ray
Kayhan Space Corp.
Eric K. Sutton, Jeffrey P. Thayer
University of Colorado Boulder
Siamak G. Hesar
Kayhan Space Corp.

1. INTRODUCTION

With multiple satellite mega-constellations, such as Spire, SpaceX's Starlink, OneWeb, and Amazon's Kuiper being planned in the LEO regime over the next decade, space traffic in the near-Earth space domain will reach unprecedented levels of congestion. Many of these planned constellations, such as Starlink, utilize automatic collision avoidance techniques for orbit safety and maintenance of their satellites. But they are still reliant on orbit data of all other satellites and debris in the neighborhood of their satellites from the 18th Space Squadron. Therefore, accurate prediction of the orbital states, and subsequently, thermospheric density, is a problem of growing significance that requires immediate attention. The effect of thermospheric density perturbations becomes especially evident in the very low earth orbit (VLEO) regime, where small uncertainties in the density predictions can dramatically impact operations, as shown by the February 2022 Starlink loss event.

The current operational density model for orbit predictions and conjunction analyses used by the Department of Defense (DOD) is the Air Force High Accuracy Satellite Drag Model (HASDM). HASDM is considered the gold standard of operational density modeling as it provides a very accurate picture of the current average state of the thermosphere by assimilating real-time tracking data from around 90 calibration objects and dynamically correcting the baseline JBH09 model (a slight variant of Jacchia Bowman 2008 or JB2008 model). But HASDM densities are only available in real-time for government users. For non-government users, there are several non-assimilating density models, such as the Mass Spectrometer Incoherent Scatter Radar (MSIS) series of models and JB2008, used in operations with no clear consensus on which model performs the best in what scenario. These models are typically biased, either high or low, with HASDM containing the least biases due to real-time data assimilation. These biases can be somewhat corrected during orbit determination during quiescent conditions, resulting in acceptable orbit fits and short-term orbit predictions. However, during extreme space weather conditions, the models fail to capture perturbations over short time scales and local spatial scales, leading to poor orbit fits and possible catalog loss. As the provision of civil SSA services transitions from the DOD to the DOC as per the Space Policy Directive - 3 (SPD-3), a commercial atmospheric density model with a performance comparable to HASDM or better will be essential for the smooth operation of civil SSA.

An accurate thermosphere forecasting system requires a model rooted in full physics of the coupling between the upper and lower atmosphere and the Sun-Earth system. Such a model would better account for local-scale and higher frequency perturbations that semi-empirical models fail to capture. To be consistent with the current average state of the thermosphere, a physics-based model needs to be continuously calibrated with real-time data ingested through a data-assimilation methodology. The planned mega-constellations discussed in the preceding paragraph can serve as

signals of opportunity for such a system with their extensive spatial and temporal coverage of the thermosphere and high-cadence GPS data. Additionally, planned science missions such as the Geospace Dynamics Constellation (GDC) will carry high-fidelity GPS receivers that can be used for high accuracy density retrievals along the orbit.

One of the first steps towards such a data-assimilative physics-based model of the thermosphere is accurate retrieval of near real-time densities. The high-cadence position and velocity information obtained from the GPS receivers can be used to retrieve estimates of neutral density along the orbital tracks of the satellites. Extensive work has been carried out in estimating atmospheric densities from GPS measurements by various groups. GPS measurements from CHAMP, GRACE, GOCE, and Swarm were used to estimate non-conservative accelerations in a reduced-dynamic POD scheme, so-called 'GPS accelerometry' [1, 2, 3].

A simplification of this method, which bypasses complex processing of the raw GPS measurements, is to use the final Precise Orbit Determination (POD) data for atmospheric density retrieval. Since the POD data are usually obtained within a few centimeters of accuracy, they can be used to estimate atmospheric densities with an accuracy comparable to processing raw GPS measurements. There are a few ways that POD can be used for this purpose. In one class of methods, they can serve as measurements in an orbit determination scheme [4, 5, 6, 7, 8], where atmospheric densities are estimated as part of the filtering framework — a sort of 'POD accelerometry'. In the second class of methods, the POD data can be used to numerically calculate orbit parameters, such as the energy dissipation rate (EDR) or the total acceleration, that contain information related to atmospheric density. EDRs derived from POD data [9] and TLEs [10] have been used to infer effective atmospheric densities over a chosen arc-length that are then further ingested in data-assimilation schemes to improve density nowcasts. The POD velocities can be numerically differentiated to obtain accelerations from which atmospheric densities can be inverted [11, 12].

All these methods have relative advantages in terms of ease of implementation and estimated density accuracy depending on various factors, such as errors in non-conservative force models, the temporal resolution of the data, and the drag signal-to-noise ratio (SNR). The drag SNR is representative of factors that determine the drag magnitude, such as the altitude, area-to-mass ratio (AMR), and space weather activity, as well as the accuracy of the POD data. To effectively derive densities for data-assimilation methods, the most appropriate method must be chosen given the satellite orbit, quality of the data, and space weather conditions. An extensive error analysis of these methods is required at different altitudes to understand their relative performances for density retrieval. This work aims to provide an understanding of the trade-offs between the methods that will aid the reader in selecting an approach for their specific application. We perform an error analysis of two approaches from the POD-based density retrieval method classes described in the preceding paragraph - POD accelerometry and EDR for the 300-800 km altitude regime. The majority of the comparative analysis is performed during solar minimum ($F_{10.7} = 72.5$). The remainder of this study provides a brief overview of the two methods and provides their sensitivity analyses for various method dependencies over the selected altitude regime.

The ultimate goal of this work is to create a long-term, continuously updated, neutral density dataset that can be ingested in a "commercial data-driven atmospheric density modeling framework." The results of the preceding error analysis are used to select the method and tuning parameters for density retrievals using data from the Spire constellation. Our results demonstrate that the outputs from density models are in better agreement with HASDM densities when calibrated by satellite tracking data.

2. METHODOLOGY

The two methods compared in this paper - POD accelerometry and EDR - make use of POD data to infer atmospheric densities along the orbital tracks of the satellites. The methods differ in their approach to ingesting and processing the POD data. In the most common form of POD accelerometry, empirical accelerations are estimated in the form of piecewise constants [1] or one cycle-per-revolution (cpr) terms [13] along each direction. These are usually estimated in a batch least-squares estimator where the terms are fixed along some orbital arc. The other approach in POD accelerometry is to model the accelerations as stochastic terms in the form of Gauss-Markov processes [8, 3] whose states are estimated in a sequential filter-smoother. This work uses a second-order Gauss-Markov process (GMP2) to model the correction to a nominal atmospheric model used in the filter. An iterated extended Kalman filter (EKF)-smoother is used that provides estimates of the density correction at each measurement step.

In EDR, the POD positions and velocities are used to calculate the change in mechanical energy of the satellites caused by the dissipation due to non-conservative forces. By assuming other forces are modeled accurately, the dissipation

due to atmospheric drag and, subsequently, the densities are calculated.

The measurements for this work - precise positions and velocities - are generated by simulating nearly circular satellite trajectories with altitudes in the 300-800 km range. The POD data are considered perfect, i.e., no errors are added to the simulated POD. The impact of POD errors on the method performance is analyzed in section 3.4. The POD data are assumed to be available every 10 s, with one day's worth of data being processed. The area-to-mass ratio (AMR) for the modeled Spire cubesat is 0.02 m^2/kg, thus putting it in the category of low AMR objects. The higher the object's AMR, the larger the density signal in the tracking data will be. Therefore, atmospheric density can be extracted with higher accuracy for high AMR objects.

The true density is modeled using HASDM data from the SET HASDM database [14]. HASDM densities are available from January 1, 2000, through December 31, 2019, that can be requested from the SET website at `spacewx.com/hasdm/`. The data covers two complete solar cycles with a 3-hour time resolution, at $10^\circ \times 15^\circ$ latitude/longitude bins and 25 km steps between 175 and 825 km. In the POD accelerometry method implemented here, a baseline model is used as part of the orbit determination process, to which corrections are estimated using POD data. NRLMSISE-00 [15] is the baseline atmospheric density model being used.

Baseline solutions for comparison purposes for both methods are generated using perfect force dynamics modeling. The degradation in solutions with force errors compared to the baseline solutions is discussed in the next section.

3. ERROR ANALYSIS

The accuracy of the retrieved densities from both methods depends on multiple factors such as truncation of the gravitational field model, errors in the other non-conservative force models, attitude, and drag-coefficient. The relative performance of the methods will depend on the nature of the error and the satellite's orbital altitude. In this section, we carry out an error analysis of the methods for the factors that have the largest effects on the density estimation accuracy, including truncation of the geopotential, mismodeling of non-conservative forces of SRP and ERP and attitude errors. Finally, we end the section with an analysis of the method performances for varying drag environments and POD accuracy. It should be noted that one of the largest errors in density retrievals is introduced as a result of uncertainties in the drag-coefficient. The nature of gas-surface interactions that determine the drag-coefficient can be quite complex. There are gaps in the knowledge of key parameters that feed into these models. The models are usually more well-constrained at lower altitudes where the nature of gas reemission from the surface is more diffuse [16]. But at higher altitudes, the nature of reemission is less understood, with fewer observations to provide any conclusive evidence [17]. This is especially true in the oxygen-to-helium transition region, which can vary significantly depending on solar activity and geographical location [18]. The uncertainties in the drag-coefficient and the consequences for retrieved densities have been extensively studied in literature [19, 8, 6]. In this work, the error introduced in the retrieved densities due to the drag-coefficient is not analyzed due to the relatively simple nature of the error relationship. The errors have almost a one-to-one relationship in the sense that a 10% error in the modeled drag-coefficient will result in a 10% error in the retrieved density for the methods considered in this paper. On the other hand, the errors due to other unmodeled forces and the attitude have a more complicated relationship to the retrieved densities.

3.1 Gravitational force modeling error

The gravitational field used for the propagation of Earth-orbiting satellites is modeled using a spherical harmonic expansion. The gravitational field potential or geopotential is given by [20]

$$U = \frac{GM_e}{r} \sum_{n=0}^{\infty} \sum_{m=0}^{n} \frac{R_e^n}{r^n} P_{nm}(\sin\phi)(C_{nm}\cos(m\lambda) + S_{nm}\sin(m\lambda)), \tag{1}$$

where G is the universal gravitational constant, M_e is the mass of Earth, r is the distance of the point from Earth's center, n is the degree and m is the order of the geopotential, R_e is the radius of Earth, P_{nm} are associated Legendre functions of the first kind, ϕ and λ are geocentric latitude and longitude, and C_{nm} and S_{nm} are spherical harmonic coefficients. The gravitational acceleration can be calculated by taking the first derivative of the geopotential with respect to the position vector and rotating to the Earth-centered inertial frame. The accuracy of the gravitational acceleration is controlled by the spherical harmonic coefficients C_{nm} and S_{nm} and the degree/order of truncation. The spherical harmonic coefficients are available in the form of numerous global gravity field models that differ from each other in the ingested data. The difference between the models is negligible for the accuracy concerned here [21].

The primary estimation errors due to the gravitational field stem from the truncation of the model. The gravitational field model in the filter is usually truncated based on orbit propagation errors and orbit fit residuals due to computational expenses [22, 23]. But when estimating non-conservative force parameters, the contribution from higher-order gravitational harmonics becomes more important. Specifically, the ignored higher-order harmonics alias into the estimated non-conservative force parameters. Ray and Scheeres (2020) [21] showed that an order 90 gravitational field at 350 km and order 50 field at 850 km would be ideal for minimizing aliasing errors into estimated cannonball drag and SRP coefficients. Therefore, it is important to understand the trade-offs between the computational complexity of using a higher-order gravitational field and errors introduced in retrieved densities from a lower-order gravitational field.

To mimic the effects of gravitational field model truncation, the true trajectory is simulated using the EGM2008 model [24], truncated at order 200. The EGM2008 model used in estimating the densities with the two methods is truncated at lower orders. The density retrieval errors for increasing orders of truncation of the gravitational field model used in the estimation methods are plotted in Fig. 1. As expected, with increasing orders of truncation, the estimated density improves accuracy. For POD accelerometry, a minimum truncation order of 80-100 is required at all altitudes for the density error to converge. This number varies quite a bit for EDR depending on the altitude. For altitudes greater than 400 km, a truncation order of 60-70 is sufficient. This is because of the larger arc-lengths at these altitudes that averages out the gravitational error. At 300 km and 400 km, the error is still decreasing at order 120. Note that for noisy POD, the errors will converge at a smaller order of truncation for EDR, similar to POD accelerometry. Though the POD accelerometry also ingests perfect POD data, noise is introduced in the system through the stochastic process used for density corrections. For 300 km-500 km, at the steady state order of truncation, EDR performs marginally better than POD accelerometry.

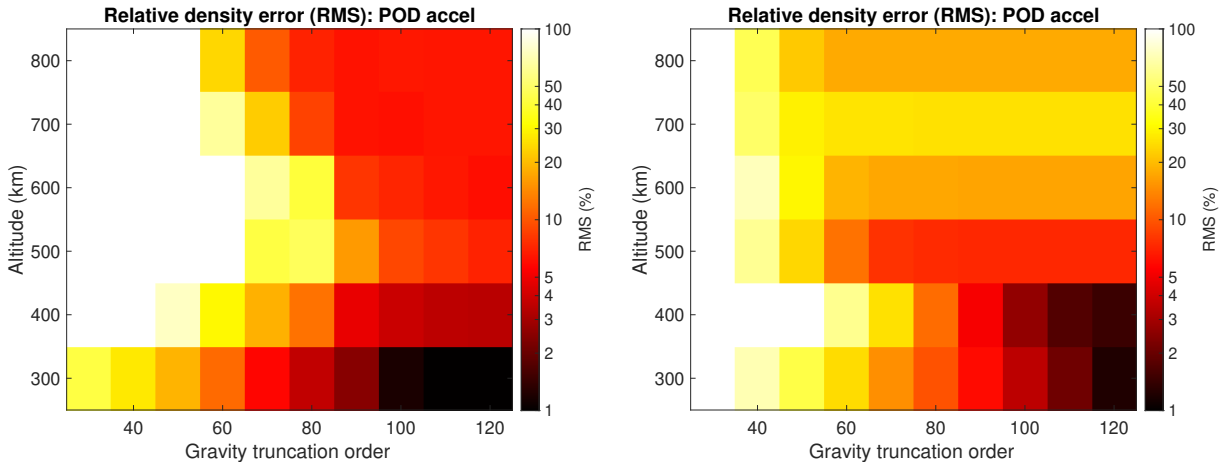

Fig. 1: Solar minimum ($F_{10.7} = 72.5, A_p = 9$): (a) RMS of relative density estimation error using POD accelerometry; (b) RMS of relative density estimation error using EDR. The color bar axis is limited to 100%.

3.2 Non-conservative force modeling errors

In deriving neutral densities from POD, there's an inherent assumption that all other non-conservative forces are accurately modeled so that their effects can be subtracted out. The remaining errors are then attributed to drag effects or more specifically, the neutral density. But modeling errors exist in other non-conservative forces and associated parameters such as SRP, ERP, thermal radiation pressure, and atmospheric winds in the drag equation that trickle down to the derived density estimates. The largest contribution comes from the SRP force followed by the ERP force. Atmospheric winds, for example, will introduce errors of a few percent in the velocity and subsequently, the retrieved densities. Therefore, it is imperative to model the SRP and ERP forces accurately. The SRP force acting on the satellite can be modeled by summing up the radiation force acting on each panel of the satellite as follows

$$\boldsymbol{a}_{SRP} = -P_s \frac{C_r}{m} \left(\frac{AU}{|\boldsymbol{r_s}|} \right)^2 f_s \sum_{k=1}^{6} A_k \cos\theta_k [(1-\rho_k)\hat{\boldsymbol{r}}_s + 2(\frac{\delta_k}{3} + \rho_k \cos\theta_k)\hat{\boldsymbol{n}}_{\boldsymbol{k}}], \tag{2}$$

where $P_s = 4.56\ \mu Pa$ is the solar radiation pressure at 1 AU distance, $\boldsymbol{r_s}$ is the satellite to Sun position vector, f_s is the shadow factor [25], A_k are the areas of the satellite surfaces with $\hat{\boldsymbol{n}}_{\boldsymbol{k}}$ as the unit vectors in the satellite body frame, θ_k are the angles that the sun vector makes with the surface unit vectors, δ_k and ρ_k are the diffuse and specular reflectivities of the surfaces respectively, and C_r is the SRP coefficient or the scaling factor in the panel model.

The ERP force, as the name suggests, is the force due to the radiation emitted from the Earth's surface. It comprises of two components - shortwave flux or albedo which is non-zero only for the illuminated areas of Earth and the re-radiated longwave flux which is emitted from all parts of the planet. In this work, we use the ERP model developed by Knocke et al (1988) [26] that divides the Earth's surface into multiple grid segments and calculates the force due to each Earth segment using historical seasonal averages of the thermo-optical properties of Earth. The effects of SRP and ERP errors on the performance of POD accelerometry and EDR method will depend on the relative magnitude of the forces compared to drag and relative energy dissipation respectively. The average acceleration magnitudes and energy dissipation over an orbit for the three forces are plotted in Fig. 2.

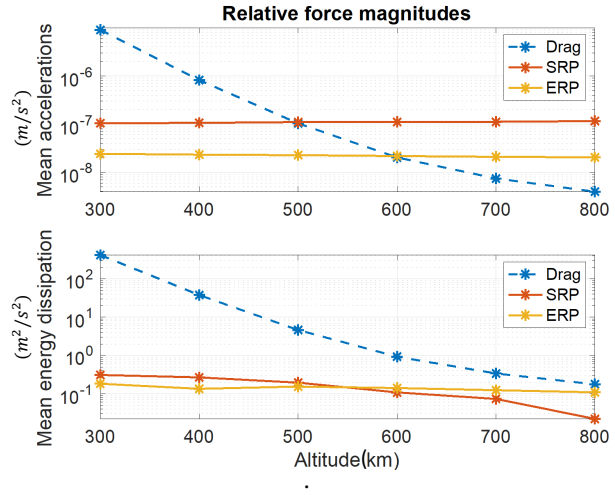

Fig. 2: Solar minimum ($F_{10.7} = 72.5, A_p = 9$): Relative magnitudes of average acceleration and energy dissipation for atmospheric drag, SRP and ERP forces for a satellite with an AMR of 0.02

First, the effect of errors in the SRP force is investigated by taking different values of the panel optical properties in the filter model than the ones used to generate the truth. In the POD accelerometry method, the errors in the SRP force can partly be compensated for by estimating SRP parameters in the filter force model. The most common way is to estimate a global scaling factor for the SRP panel model [3], C_r in Eq. 2. But a single scaling factor might not work very well if the satellite attitude with respect to the sun-satellite line is changing. McMahon and Scheeres (2015) [27] proposed the Three-constants model that estimates scaling factors along three perpendicular inertial directions -

$$\boldsymbol{a}_{SRP} = \frac{K}{r^2}[A_0\hat{\boldsymbol{u}} + A_1\hat{\boldsymbol{v}} + A_2\hat{\boldsymbol{w}}] \tag{3}$$

where K is a constant, $\hat{\boldsymbol{u}}$ is the unit vector from the Earth to the Sun, $\hat{\boldsymbol{w}}$ is in the direction of the angular momentum of Earth's heliocentric orbit and $\hat{\boldsymbol{v}}$ completes the triad. The spacecraft-Sun unit direction is considered to be almost equal to the Earth-Sun direction. A_0, A_1 and A_2 are constants to be determined. If only the component in the direction of the Sun is taken, it reduces to the cannonball model. For the EDR method, there's no way to correct for errors in other non-conservative forces since no estimation is being performed. But the relative contribution of SRP and ERP to the energy dissipation is smaller than the drag force for all altitudes as seen in Fig. 2.

The relative density error statistics using POD accelerometry and EDR method with SRP modeling errors are plotted in Fig. 3. For the POD accelerometry in Fig. 3 (a), the density errors are compared for an estimated SRP scaling factor and the SRP Three-constants model. As can be seen in Fig. 3, the errors in the retrieved densities with a global scaling factor estimated for SRP is significantly larger than the Three-constants model at altitudes greater than 400 km. A single scaling factor cannot compensate for biases in the SRP force model. The Three-constants model will be used in the filter in subsequent sections.

For the EDR method in Fig. 3 (b), the density errors are compared with the baseline solution generated with perfect force models. At altitudes less than 500 km, the errors are negligible. The errors increase up to 600 km and then start decreasing again due to the averaging arc-length being close to an orbit at 700 km and 800 km. This leads to the SRP errors averaging out; subsequently, the density estimates are close to the baseline solution. Therefore, with more significant SRP errors, selecting an averaging arc-length of at least one complete orbit for higher altitudes might be more advantageous. Interestingly, the mean of the density error is smaller than the baseline solution. This implies that the SRP error averaged over the given arc-length somehow compensates for the average error in the density estimate. The ERP force is around 20% of the SRP force and is primarily in the radial direction. Therefore, the effects of

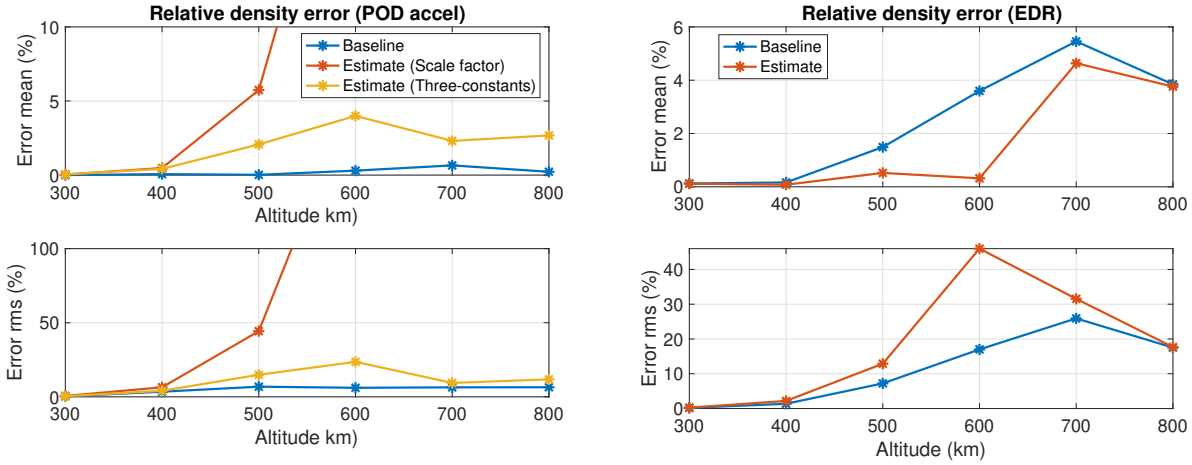

Fig. 3: Solar minimum ($F_{10.7} = 72.5$, $A_p = 9$): Relative density estimation errors for SRP modeling errors in the filter with (a) POD accelerometry and (b) EDR method. The y-axis is limited to 10% mean and 100% RMS for POD accelerometry.

ERP on the derived densities will be small for lower altitudes. ERP errors are introduced in the filter using a high-fidelity model that uses monthly-averaged radiation flux data from the Clouds and the Earth's Radiant Energy System (CERES) instrument [28]. The filter uses the Knocke et al. model [26] that divides the Earth into multiple rings (six, in this work) and uses historical seasonally averaged data for the radiation fluxes for each ring. A global scaling factor is estimated for the ERP force in the POD accelerometry method. The estimated density errors for both methods are plotted in Fig. 4. For POD accelerometry, the errors due to ERP slightly degrade the accuracy of the estimated densities at altitudes higher than 500 km due to the low drag signal. For EDR, errors in ERP do not contribute to the estimated densities. To minimize the errors due to ERP, a model that accounts for current Earth radiation fluxes should be used, such as the extended model developed by Vielberg and Kusche (2020) [29] that uses hourly data from the CERES instrument [28]. Additionally, estimating a global scaling factor improves the results as well.

3.3 Attitude errors

The attitude of a satellite plays a key role in neutral density retrieval. The attitude affects the cross-sectional area in the ram-facing direction, which in turn determines the magnitude of the drag force acting on the satellite. Therefore, errors in the attitude directly affect the retrieved densities through the cross-sectional area or the ballistic coefficient. Additionally, attitude information is required to model SRP and ERP forces accurately. Due to attitude errors, force modeling errors in SRP and ERP contribute to secondary effects in the density retrieval accuracy.

The errors in attitude are simulated by adding a constant bias in the roll, pitch, and yaw directions. At lower altitudes, the dominant source of error is the drag-coefficient. For example, at 300 km, the relative error in the density is similar to the relative error in the drag-coefficient and therefore, not shown here. A maximum error of around 10% is seen in the drag-coefficient and, consequently, the estimated densities for a bias in the pitch/yaw of 10 degrees. But at 800 km, the errors in the densities are much larger though the drag-coefficient errors remain the same, as can be seen in Fig. 5. The resulting SRP and ERP errors dominate the retrieved densities' accuracy at this altitude. With POD accelerometry, the errors can be constrained by estimating force scaling factors similar to the previous section. The estimated parameters absorb the errors introduced due to attitude and improve the accuracy of the retrieved densities. A global scaling factor is estimated for ERP, and the Three constants model is used for SRP in Fig. 5.

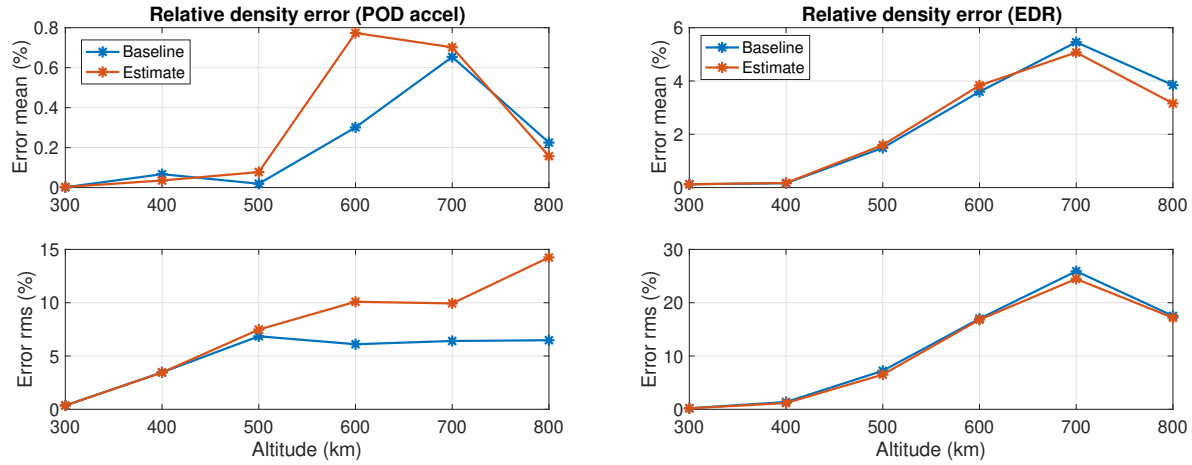

Fig. 4: Solar minimum ($F_{10.7} = 72.5, A_p = 9$): Relative density estimation errors for ERP modeling errors in the filter with (a) POD accelerometry and (b) EDR method.

3.4 POD accuracy in different drag environments

The accuracy of the available POD can vary depending on the method employed — kinematic, dynamic, or reduced-dynamic, type of tracking data, and measurement noise. In highly precise science missions, an accuracy of a few centimeters in position and tens of micrometers per second is commonly achieved [13, 30, 31]. In commercial satellites with scientific data products such as Spire, POD accuracy of tens of centimeters in position and a few hundred micrometers per second is reported [32]. For most other satellites, where orbit accuracy is not critical, the accuracy of orbit solutions can be at the order of meters or more and might not even classify as POD anymore. Up until this point in our analysis, the POD data have been treated as ideal, with no errors. This section investigates the impact of POD errors on density accuracy.

The measurement noise is usually modeled as white Gaussian noise in the estimation methods employed in orbit determination. Therefore, errors in the POD are introduced using a white noise process with a specified RMS value. It should be noted that the POD errors obtained from the orbit determination will not remain Gaussian due to the nonlinearity of orbital dynamics. Since POD data are obtained by processing raw, noisy measurements (where Gaussianity of the noise is a more accurate approximation) in an orbit determination framework, the errors in POD may become more systematic than stochastic, with correlation to errors in the orbital dynamics model and measurement biases. The errors in POD may also vary during the data-arc so that the POD may be more accurate in certain parts of the arc than others. But assuming the POD errors to be Gaussian is a good first-order approximation, and the results provide a rule-of-thumb for the relative performances of the techniques in different drag regimes. Modeling the nature of the POD errors can become quite complex [33] and is not addressed in this work. Introducing noise in the POD changes the arc-lengths that minimize the density error using EDR. Therefore, the arc-lengths for perfect POD in Fig. **??** will no longer apply to noisy POD measurements. In order to compare the EDR results for different POD noise levels, the arc-lengths that minimize the density error RMS at each POD noise level are selected.

The density retrieval accuracy strongly depends on the drag SNR, which is a function of the POD noise level, altitude, space weather conditions, and the satellite AMR. In order to determine the accuracy of retrieved densities that can be expected with either method, it is more informative to use the drag acceleration magnitude as a metric to represent the drag regime instead of analyzing each of the parameters separately. Therefore, the altitude ($300-800\ km$), AMR ($0.01-10$), and space weather conditions ($F10.7 = 72-280$, $A_p = 9-203$) are varied to obtain a plausible range of drag acceleration magnitudes encountered in orbit. The densities obtained with the two methods are compared for the range of drag acceleration magnitudes with POD data of varying accuracy (1 cm - 50 cm). The velocity noise level is assumed to be 1/(1000 s) of the position noise level. The error RMS of the retrieved densities are plotted in Fig. 6 for both methods. For low SNR regimes ($< 10^{-6}\ m/s^2$ drag and $> 0.25\ m$ POD noise), the errors render the estimated instantaneous densities unusable for both methods, though the "high-error regions" stretch larger for EDR. In these regions, the averaging length required for EDR quickly increases leading to a loss of geophysical information. Since we are comparing the retrieved densities to the instantaneous true density, the errors for EDR are expected to be larger

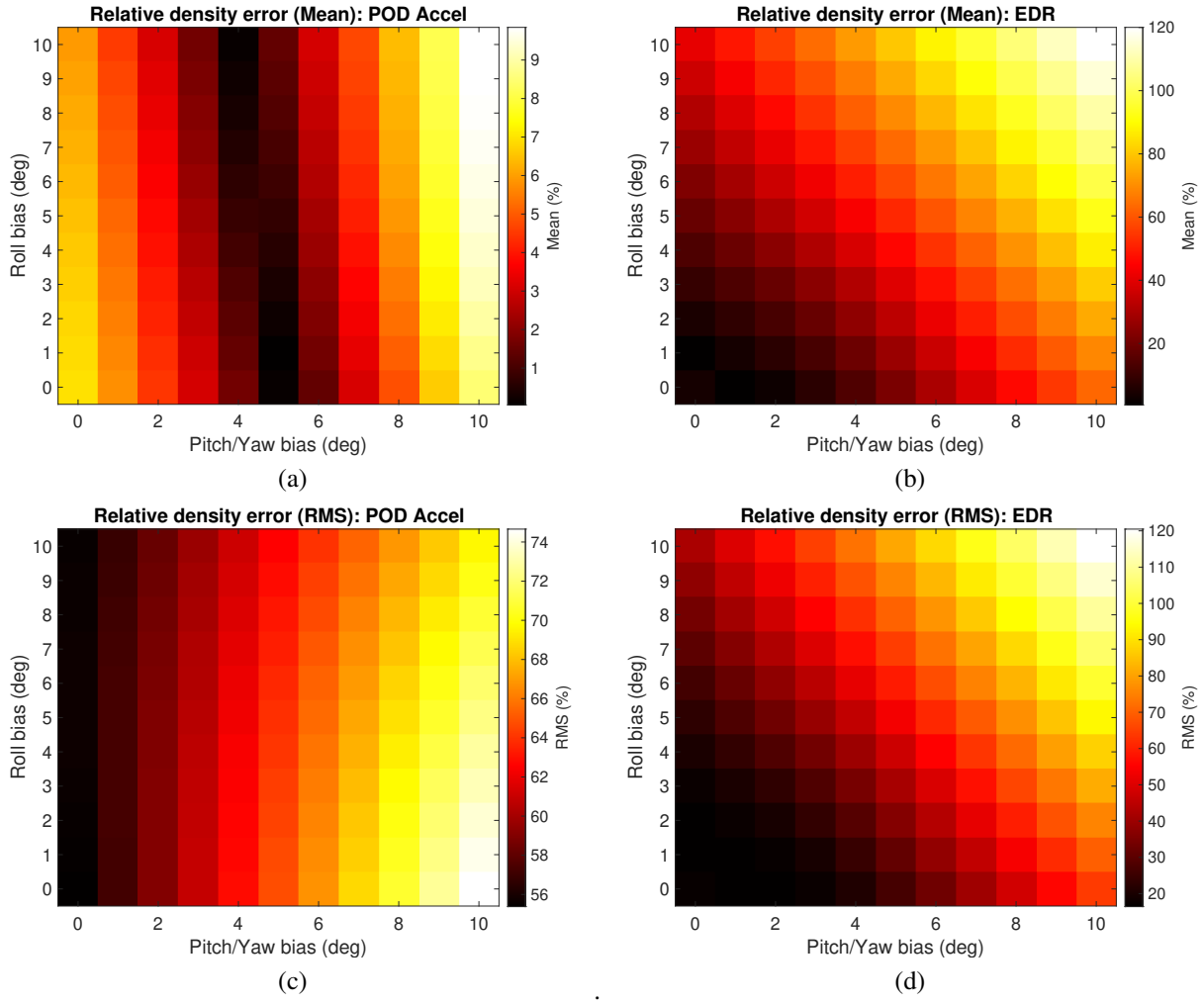

Fig. 5: Solar minimum ($F_{10.7} = 72.5$, $A_p = 9$): Mean and RMS of relative density estimation error with (a),(c) POD accelerometry and (b),(d) EDR method at 800 km. The upper panel shows the error mean for the two methods while the lower panel shows the RMS. Three-constants model is used for SRP and a global scaling factor is estimated for ERP with POD accelerometry

than POD accelerometry. Some typical satellite scenarios are shown in the signal-noise plot as described in Table 1. Starlink satellites are launched at a lower parking orbit and then boosted to operational altitudes of around 550 km. At the parking orbit, the solar panels are kept tangential to the atmosphere in an open-book configuration while at the operational altitudes, the solar panels may assume an orientation perpendicular to the relative velocity vector (shark-fin configuration). The noise in the orbit determination solutions for Starlink is observed to be relatively larger, and therefore the Starlink scenarios are placed at the top of the plot. An overlap analysis of the Spire POD arcs reveals the noise RMS to be around 10 cm [34]. The POD accuracy for science missions like GRACE and GOCE is typically in the order of a few centimeters [35, 36].

Case	Space weather activity	Perigee altitude	AMR
Starlink 1	F10.7 = 127, Ap = 52 (G1 storm)	550 km (Operational orbit)	0.005 (Open-book configuration)
Starlink 2	F10.7 = 280, Ap = 203 (G5 storm)	550 km (Operational orbit)	0.05 (Shark-fin configuration)
Starlink 3	F10.7 = 127, Ap = 52 (G1 storm)	210 km (Parking orbit)	0.005 (Open-book configuration)
Starlink 4	F10.7 = 280, Ap = 203 (G5 storm)	210 km (Parking orbit)	0.005 (Open-book configuration)
Spire 1	F10.7 = 127, Ap = 52 (G1 storm)	475 km	0.02
Spire 2	F10.7 = 280, Ap = 203 (G5 storm)	475 km	0.02
GRACE	F10.7 = 127, Ap = 52 (G1 storm)	470 km	0.002
GOCE	F10.7 = 127, Ap = 52 (G1 storm)	350 km	0.0008

Table 1: Description of representative satellites in the drag signal-noise plots of Figs. 6 and 7

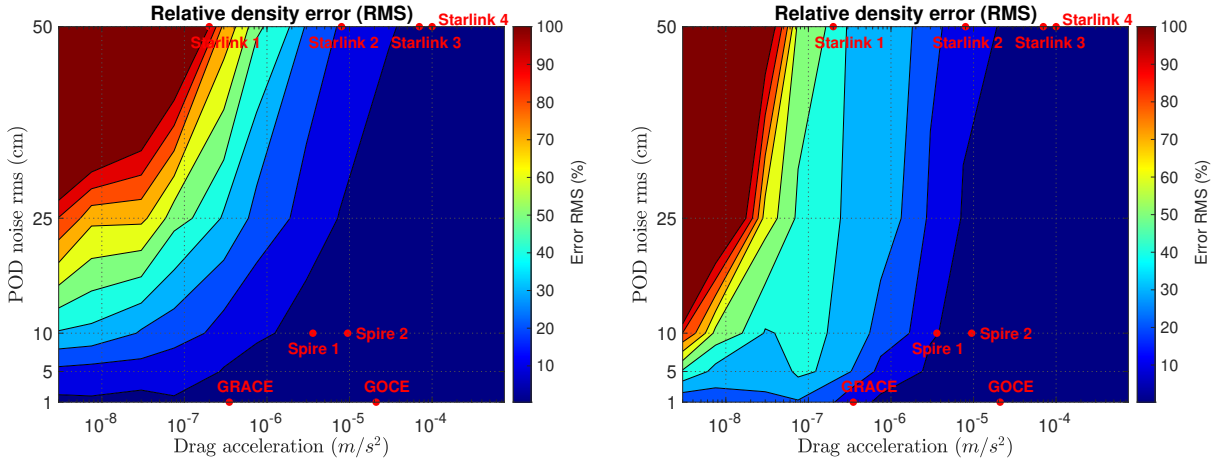

(a) (b)

Fig. 6: RMS of relative density estimation error for varying drag regimes and POD noise levels using (a) POD accelerometry and (b) EDR method. The arc-length of the EDR method is chosen for each altitude such that the error RMS is minimized. The color scale is capped at 100%. The representative scenarios for different satellites are described in Table 1

Since the density estimates obtained using EDR are averaged over a chosen time interval, some of the error in the density estimates obtained is due to averaging or the loss of geophysical information. Therefore, comparing the averaged density estimates with the instantaneous true densities at measurement cadence (typically, 1-10 s) yields poor results for EDR. Even in the case of POD accelerometry, providing density corrections to the baseline model at measurement cadence is not physically meaningful in low-drag SNR regimes. This is evidenced by the large errors between the density estimates and the true instantaneous densities seen at measurement cadence (10 s) in Fig. 6 for low SNR regions. In many applications, such as data-assimilation techniques for density modeling, an accurate average density over a given time interval is sufficient. However, one would ideally want the time interval to be small to capture geophysical variations. Therefore, it is useful to compare the minimum averaging arc-lengths for the two methods for which the density can be obtained with a given accuracy. The arc-lengths for which the density can be obtained with

10% RMS accuracy are plotted in Fig. 7. It is immediately noticeable that a good portion of the signal-noise region is missing in the EDR plot; this simply means that EDR cannot estimate average densities better than 10% within the maximum averaging arc-length of 20 hours that was used in this study. In addition, the EDR technique is able to estimate densities better than 10% for drag accelerations less than 10^{-8} m/s^2 for averaging lengths of 10-16 hours but only for noise levels of 5 cm. On the other hand, POD accelerometry can provide average densities within 10% accuracy for all the drag SNR regimes investigated here, with a maximum arc-length of 8 hours for the lowest SNR region. Given the ease of implementation and simple tuning process (selecting an averaging arc-length), EDR proves to be a viable option when retrieving densities in the high SNR regions ($> 10^{-6}$ m/s^2 drag acceleration and < 2.5 *cm* POD position noise). For lower SNR regions, POD accelerometry should be used to obtain densities with shorter arc-lengths.

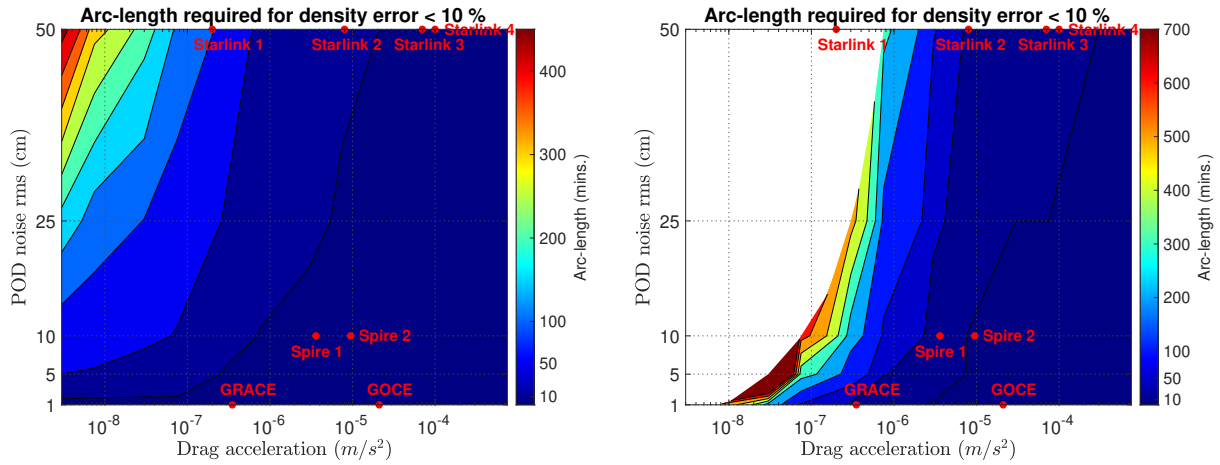

Fig. 7: Averaging arc-lengths required to obtain density errors with less than 10% error using (a) POD accelerometry and (b) EDR method. Note that arc-lengths up to 20 hours were investigated for a day's worth of processed data. The representative scenarios for different satellites are described in Table 1

4. DENSITY ESTIMATES USING REAL POD DATA

In this section, real POD data from the Spire constellation is used to estimate atmospheric densities along the orbital tracks of the Spire satellites. Two sources of Spire POD data are used in this work - 1) Spire's own internally processed POD data, available through the NASA Commercial Smallsat Data Acquisition (CSDA) Program (`earthdata.nasa.gov/esds/csdap`). The POD data is available at a per-second cadence.

2) An updated POD dataset processed by the University Corporation for Atmospheric Research (UCAR) (`https://data.cosmic.ucar.edu/gnss-ro/spire/noaa/nrt/`), hereon referred to as UCAR POD. The data is available at a per-minute cadence.

Both datasets have data-gaps depending on the duty cycle of the onboard GPS receiver. The newer satellites with satellite IDs > 99 have duty cycles approaching 80-90 %. Spire also publishes their satellite attitude in the form of quaternions. The attitude information is available at a 15-minute cadence, interpolated to 10 s intervals using Spherical Linear IntERPolation (SLERP) [37]. The POD datasets from Feb 5, 2022, are used in this analysis. POD data for 27 satellites are available through Spire's internal POD, while 15 of those satellites have POD data through UCAR as well.

An estimate of the POD errors can be obtained by comparing orbit overlaps, i.e., overlapping arcs of POD data. An example of orbit overlaps for both datasets is plotted in Fig. 8. The RMS values of orbit overlap differences are plotted for all the available satellites in Fig. 9. The RMS values of differences between the Spire and UCAR POD data, at common time-stamps (not interpolated) are also plotted in the figure. The orbit overlap errors seem to indicate that the UCAR-processed POD data contain larger errors than Spire's internally processed PODs. The POD data differences

between the two datasets are large enough to cause differences in retrieved densities.

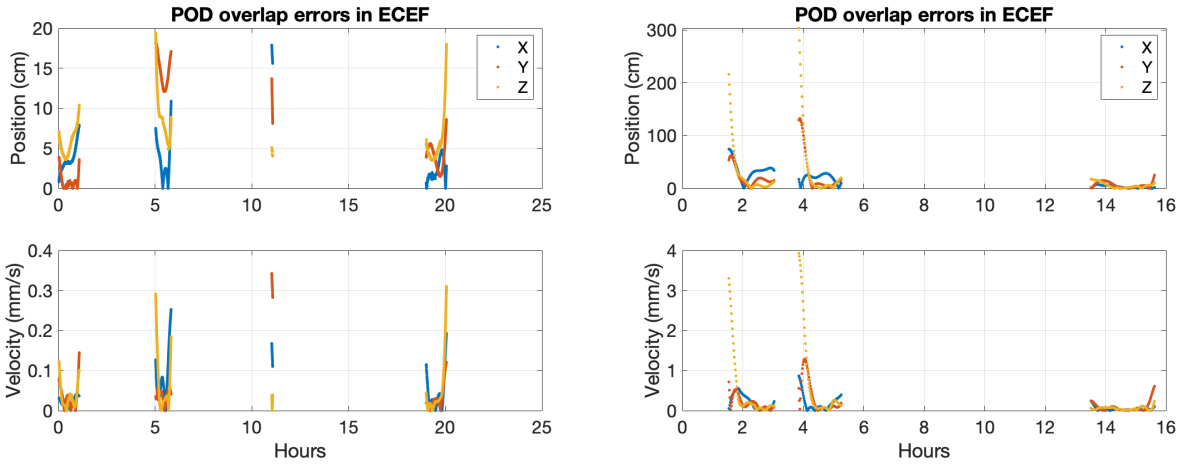

(a) (b)

Fig. 8: Orbit overlaps for (a) Spire internal POD and (b) UCAR POD for Feb 5, 2022

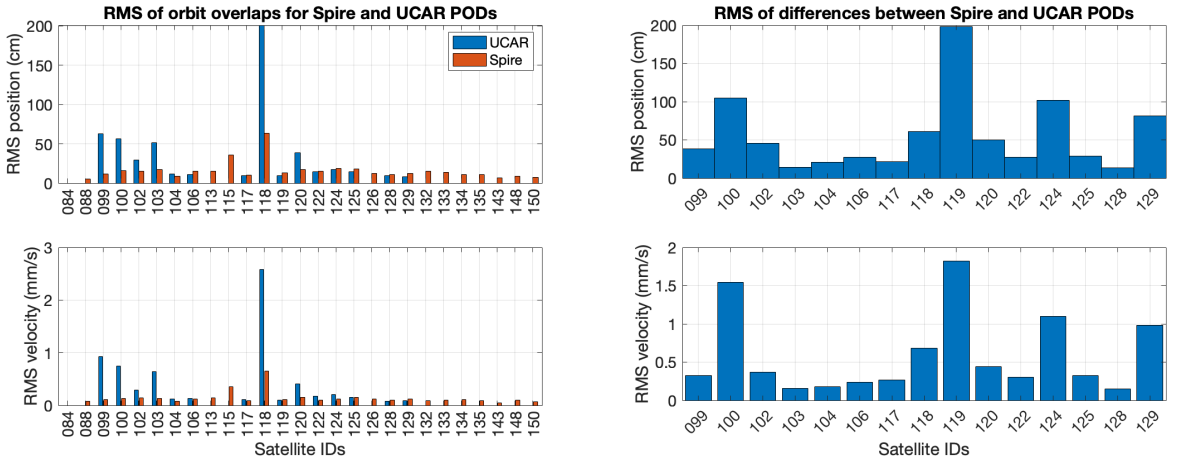

(a) (b)

Fig. 9: (a) RMS values of orbit overlap differences for both datasets, (b) RMS values of POD differences between Spire and UCAR for Feb 5, 2022

The error analyses in the preceding sections indicate that POD accelerometry can provide accurate densities at shorter averaging arc-lengths compared to EDR in low-drag SNR environments. Since some Spire satellites are at an altitude of around 580 km, and the Spire POD noise can be up to 50 cm RMS, as seen in Fig. 9, POD accelerometry is used to process the datasets. JB2008 is used as the baseline density model to which corrections are estimated using the POD data. HASDM densities are used as the ”truth” source for comparison. The estimated densities are averaged at an orbital cadence whenever a full orbital arc is available. All other arcs are ignored. A moving window average is used to obtain an averaged density at every time-step of the data (excluding the end of the data-arcs). In order to compare the densities obtained using Spire and UCAR data, the Spire data are used at a minute cadence, and only the 15 satellites common to both datasets are used. The estimated density errors compared to HASDM are binned by altitude levels and plotted in Fig. 10. The estimated densities are closer to HASDM at 450 and 550 km than JB2008 for both datasets. But at 500 km, the errors are slightly larger compared to JB2008. The densities estimated with the Spire POD data are slightly closer to HASDM than those estimated with UCAR POD data. Any differences in estimated densities due to different POD noise levels are essentially washed out at an averaging arc-length of an orbit.

However, it should be noted that a fair comparison of the estimated densities from the two datasets is complicated because the POD data from the two sources are not the same length or at the same time stamps.

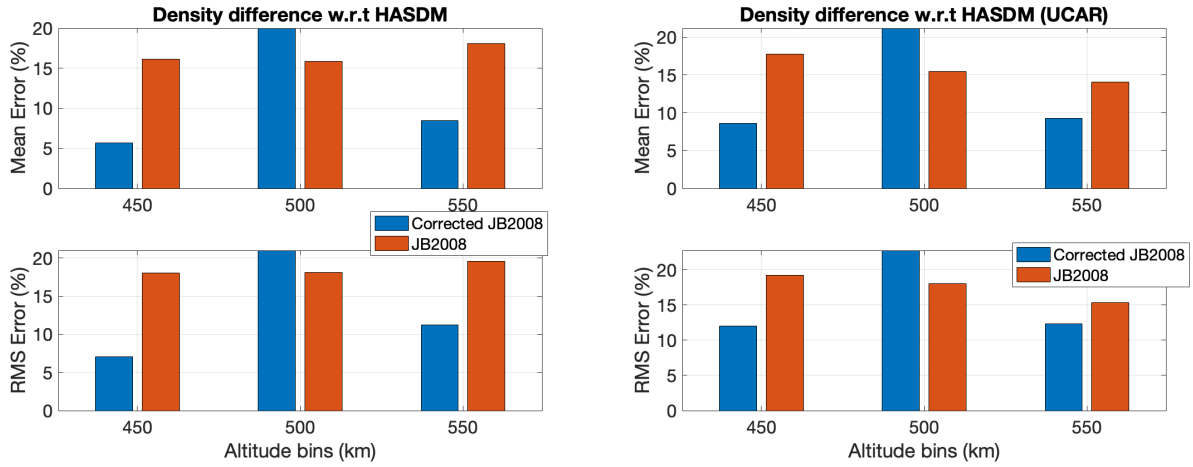

(a) (b)

Fig. 10: Mean and RMS of estimated density errors compared to HASDM with the (a) Spire POD data and (b) UCAR POD data for Feb 5, 2022

If all the 27 satellites for which Spire internal POD is available are processed, the estimated densities at 500 km are closer to HASDM, as seen in Fig. 11. The errors in daily averaged densities are much smaller, as seen in Fig. 11 (b), which implies the errors can be further reduced by increasing the averaging length. The data above 600 km is scarce; therefore, the corrections to the baseline model are limited.

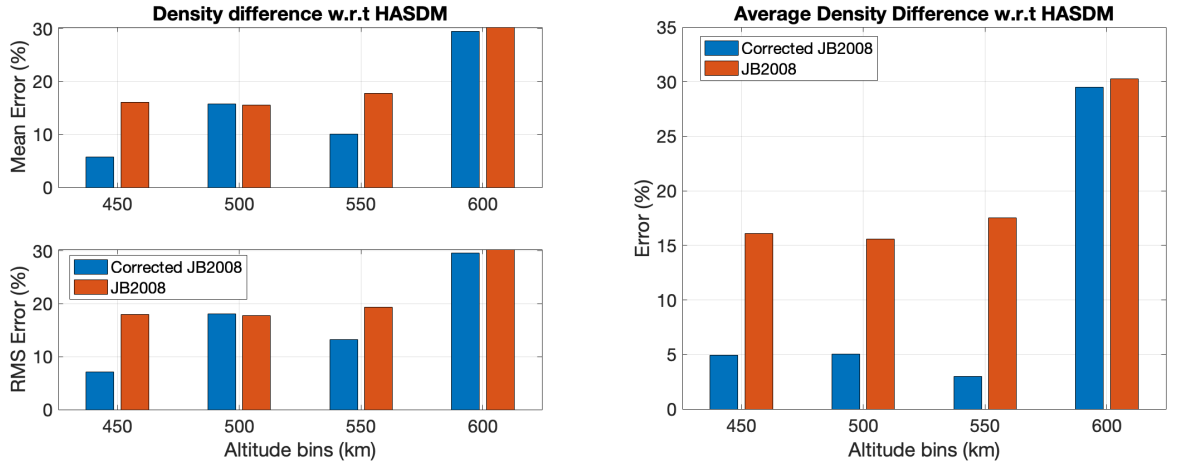

(a) (b)

Fig. 11: (a) Mean and RMS of estimated density errors compared to HASDM at an orbital cadence with the Spire POD data and (b) Error in the daily-averaged density for Feb 5, 2022, using 27 satellites

5. CONCLUSIONS

In this paper, we explored two classes of methods using Precise Orbit Determination (POD) - 1) processing tracking data in an orbit determination scheme (POD accelerometry) and 2) using the tracking information directly to calculate densities (Energy Dissipation Rate (EDR)). Their sensitivities to various possible errors across the 300-800 km altitude

regime during solar minimum conditions ($F_{10.7} = 72.5$) were compared to understand the applicability of each method in different scenarios.

Both methods are sensitive to errors in the dynamics models. SRP and ERP model errors have a smaller effect on the EDR-derived densities than POD accelerometry. This is because the integral of the EDR due to SRP or ERP over a data-arc may approximately average out, in contrast to the drag EDR. Therefore, depending on the orbital regime and chosen data-arc, the energy dissipation due to SRP and ERP may essentially be ignored. Though the POD accelerometry results are more sensitive to errors in the SRP and ERP models, a significant portion of the error may be mitigated by estimating scale factors for the forces. Choosing the appropriate force parameters to estimate for POD accelerometry is important, as Fig. 3 demonstrates. Similarly, for errors in attitude, the resulting errors in the SRP and ERP forces can be reduced by estimating appropriate scale factors for POD accelerometry. Note that one of the most dominant error sources, i.e., the drag-coefficient has not been considered directly in this work due to the almost one-to-one relationship of their error correlations (nearly one). On the other hand, the errors due to other unmodeled forces and the attitude have a more complicated relationship to the retrieved densities, and this work sought to provide more insight into their nature.

For perfect POD, i.e., without any errors, EDR works as well as POD accelerometry until around 500 km. But EDR degrades in accuracy at low drag SNR regimes, as shown in Fig. 6. Comparatively, POD accelerometry is less sensitive to POD noise since it processes the POD in a filtering framework. The main advantage of EDR lies in the ease of implementation and simplicity of the setup required to obtain the densities. There are fewer tuning knobs for EDR compared to POD accelerometry. The loss of geophysical information or averaging error introduced in the EDR estimates will be reduced for satellites that are in near-circular terminator orbits or where the variations due to eccentricity balance out the day-night variations in density. EDR is a viable option for density retrieval for high drag SNR regimes, i.e., for high cadence and low-noise POD solutions at lower altitudes, high solar activity, and high AMR satellites. But for low-drag SNR regions, POD accelerometry should be used to retrieve densities to retain more geophysical information in the density.

POD accelerometry was used to estimate densities using real POD data from the Spire constellation. The densities estimated at orbital cadence from two POD sources of different fidelity - Spire internally processed POD data and UCAR processed POD data - were compared. At orbital cadence, the errors in estimated densities compared to HASDM were similar for both sources, using the 15 satellites common to both datasets. The differences would be more evident if the densities were estimated at a higher cadence. The corrected densities are closer to HASDM than the baseline model (JB2008) at 450 and 550 km but show some degradation in accuracy at 500 km. But including all 27 satellites for which Spire POD data are available improves the errors. The daily-averaged densities are much closer to HASDM than the baseline JB2008.

The long-term goal of this project is to provide the community with an atmospheric model calibrated in near real-time with tracking data from satellite constellations. The results of this study indicate the potential of using POD data from commercial satellites to provide accurate density estimates. We are currently using POD accelerometry and EDR to obtain neutral density estimates over several years using POD data from commercial constellations like Spire and Starlink. These estimates can eventually be ingested in a data-assimilation framework to obtain a calibrated atmospheric density model.

6. ACKNOWLEDGEMENTS

This material is based upon work supported by the National Aeronautics and Space Administration under Grant 80NSSC21K1554 issued through the Heliophysics Division Space Weather Science Application initiative. Part of the work was initiated through a previous Air Force STTR Phase 2 award No. FA864921P1517, in collaboration with Space Environment Technologies (SET). We sincerely thank Dr. W. Kent Tobiska, Dr. Shaylah Mutschler from SET, and Dr. Erik Blasch, Program Officer at AFOSR, for their support. We are grateful to Spire for providing information on their spacecraft properties for this effort.

7. REFERENCES

[1] J.V.D. Ijssel and Pieter Visser. Performance of GPS-based accelerometry: CHAMP and GRACE. *Advances in Space Research*, 39, 2007.

[2] P.N.A.M Visser and J.A.A. van den Ijssel. Orbit determination and estimation of non-gravitational accelerations for the GOCE reentry phase. *Advances in Space Research*, 58, 2016.
[3] J.V.D. Ijssel, Eelco Doornbos, Elisabetta Iorfida, Gunther March, Christian Siemes, and Oliver Montenbruch. Thermosphere densities derived from Swarm GPS observations. *Advances in Space Research*, 65, 2020.
[4] C. A. McLaughlin, A. Hiatt, and T. Lechtenberg. Precision Orbit Derived Total Density. *Journal of Spacecraft and Rockets*, 48(1):166–174, 2011.
[5] Craig A McLaughlin, Travis Lechtenberg, Eric Fattig, and Dhaval Mysore Krishna. Estimating density using precision satellite orbits from multiple satellites. *The Journal of the Astronautical Sciences*, pages 85–101, 2012.
[6] Craig A McLaughlin and B.S. Hiatt, A Bieber. Comparison of total density derived from CHAMP precision orbits and CHAMP accelerometers. *Advances in the Astronautical Sciences*, (AAS 08-177):1193–1206, 2008.
[7] Craig A McLaughlin and B.S. Hiatt, A Bieber. Deriving density estimates using CHAMP precision orbit data from for periods of high solar activity. *Advances in the Astronautical Sciences*, (AAS 09-104):23–42, 2009.
[8] Vishal Ray, Daniel J. Scheeres, Suood Alnaqbi, W. Kent Tobiska, and Siamak G. Hesar. A Framework to Estimate Local Atmospheric Densities With Reduced Drag-Coefficient Biases. *Space Weather*, 20(3), 2022.
[9] E.K. Sutton, Jeffrey P. Thayer, Marcin D. Pilinski, Shaylah P. Mutschler, Thomas E. Berger, Vu Nguyen, and Dallas Masters. Toward Accurate Physics-Based Specifications of Neutral Density Using GNSS-Enabled Small Satellites. *Space Weather*, 19(6), 2021.
[10] M.D. Pilinksi, G. Crowley, M. Seaton, and E.K. Sutton. Dragster: An Assimilative Tool for Satellite Drag Specification. In *Advanced Maui Optical Surveillance and Space Technologies Conference (AMOS)*, 2019.
[11] Andres Calabia and Shuanggen Jin. Thermospheric density estimation and responses to the March 2013 geomagnetic storm from GRACE GPS-determined precise orbits. *Journal of Atmospheric and Solar-Terrestrial Physics*, 154:167–179, 2017.
[12] Andres Calabia and Shuanggen Jin. Upper-Atmosphere Mass Density Variations From CASSIOPE Precise Orbits. *Space Weather*, 19(4), 2021.
[13] T.C. Thomas, S.B. Luthcke, T.A. Pennington, J.B. Nicholas, and D.D. Rowlands. ICESat-2 Precision Orbit Determination. *Earth and Space Science*, 8(4), 2021.
[14] K.W. Tobiska, B.R. Bowman, D. Bouwer, A. Cruz, K. Wahl, M. Pilinski, P.M. Mehta, and R.J. Licata. The SET HASDM density database. *Space Weather*, 2021.
[15] J.M. Picone, A.E. Hedin, D.P. Drob, and A.C. Aikin. NRLMSISE-00 Empirical Model of the Atmosphere: Statistical Comparisons and Scientific Issues. *Journal of Geophysical Research*, 107(A12):2035–2051, 2002.
[16] Kenneth Moe and Mildred M. Moe. Gas Surface Interactions and Satellite Drag Coefficients. *Planetary and Space Science*, 53(8):793–801, 2005.
[17] I.K. Harrison and J.J. Swinerd. A free molecule aerodynamic investigation using multiple satellite analysis. *Planetary and space science*, 44(2):171–180, 1996.
[18] Valerie Bernstein, Marcin Pilinski, and Delores Knipp. Evidence for Drag Coefficient Modeling Errors near and Above the Oxygen-to-Helium Transition. *Journal of Spacecraft and Rockets*, 57(6), 2020.
[19] Piyush M. Mehta, Smriti N. Paul, Nicholas H. Crisp, Philip L. Sheridan, Christian Siemes, Günther March, and Sean Bruinsma. Satellite drag coefficient modeling for thermosphere science and mission operations. *Advances in Space Research*, 2022.
[20] Olliver Montenbruck and Eberhard Gill. *Satellite Orbits: Models, Methods and Applications*, chapter 3.2. Springer, 2000.
[21] Vishal Ray and Daniel J. Scheeres. Gravitational Force-Model Aliasing with Non-Gravitational Force Coefficients in Dynamic Prediction. *Journal of Guidance, Control and Dynamics*, 43(10):1984–1997, 2020.
[22] D.A. Vallado. An analysis of state vector propagation using different flight dynamics programs. *Advances in the Astronautical Sciences*, 121, 2005. Proceedings of the 15th AAS/AIAA Space Flight Mechanics Meeting, Copper Mountain, CO, January 23–27 2005.
[23] W.N. Barker, W.J. Casali, and R.N. Wallner. Earth gravitational error budget for space control. *Advances in the Astronautical Sciences*, 93:351–370, 1996. Proceedings of AAS/AIAA Spaceflight Mechanics Meeting, Austin, TX, February 12-15, 1996.
[24] Nikolaos K. Pavlis, Simon A. Holmes, Steve C. Kenyon, and John K. Factor. The development and evaluation of the Earth Gravitational Model 2008 (EGM2008). *Journal of Geophysical Research*, 2012.
[25] Olliver Montenbruck and Eberhard Gill. *Satellite Orbits: Models, Methods and Applications*, chapter 3. Springer, 2000.
[26] P.C. Knocke, J.C. Ries, and B.D. Tapley. Earth Radiation Pressure Effects on Satellites. In *Astrodynamics*

Conference, number 88-4292-CP, 1988.
[27] Jay W. McMahon and Daniel J. Scheeres. Improving Space Object Catalog Maintenance Through Advances in Solar Radiation Pressure Modelling. *Journal of Guidance, Control, and Dynamics*, 38(8):1366–1381, 2015.
[28] Bruce A. Wielicki, Bruce R. Barkstrom, Edwin F. Harrison, Robert B. Lee III, Louis G. Smith, and John E. Cooper. Clouds and the Earth's Radiant Energy System (CERES): An Earth Observing System Experiment. *Bulletin of the American Meteorological Society*, 77(5), 1996.
[29] Kristin Vielberg and Jurgen Kusche. Extended forward and inverse modeling of radiation pressure accelerations for LEO satellites. *Journal of Geodesy*, 94(43), 2020.
[30] K Zang, P Nagel, and Pastor R. Precise Orbit Determination for GRACE. *Advances in Space Research*, 31(8), 2003.
[31] J. Van Den Ijssel, P. Visser, and E. Patino Rodriguez. CHAMP Precise Orbit Determination using GPS data. *Advances in Space Research*, 31(8), 2003.
[32] Chase Brown, Jason Stauch, and Shiva Iyer. Multi-source resident space object state validation and fusion. In *IAA-UT Space Traffic Management Conference*, number IAA-UT-STM-03-01, 2020.
[33] P. Kuchynka, M. Martin Serrano, K. Merz, and J. Siminski. Uncertainties in GPS-based operational orbit determination: A case study of the Sentinel-1 and Sentinel-2 satellites. *The Aeronautical Journal*, 124(1276), 2020.
[34] Chase Brown, Jason Stauch, and Shiva Iyer. Multi-source resident state object validation and fusion. In *IAA-UT Space Traffic Management Conference*, 2020.
[35] Z Kang, P Nagel, and R Pastor. Precise orbit determination for GRACE. *Advances in Space Research*, 31(8):1875–1881, 2003.
[36] Heike Bock, Adrian Jäggi, Gerhard Beutler, and Ulrich Meyer. GOCE: precise orbit determination for the entire mission. *Journal of Geodesy*, 88:1047–1060, 2014.
[37] Ken Shoemake. Animating rotations with quaternion curves. In *SIGGRAPH '85: Proceedings of the 12th annual conference on Computer graphics and interactive techniques*, pages 245–254, 1985.